Tailoring the hole-injection layer in organic light-emitting devices by introducing Au@SiO_2 nanoparticles

Qing Lou,[1,3] Wenyu Ji,[1,*] Qinghui Zeng,[1] and Dandan Zhang[2,4]

[1]*State Key Laboratory of Luminescence and Applications, Changchun Institute of Optics, Fine Mechanics and Physics, Chinese Academy of Sciences, Changchun 130033, China*

[2]*Jiangsu Key Laboratory for Carbon-Based Functional Materials and Devices, Institute of Functional Nano and Soft Materials (FUNSOM), Soochow University, Suzhou 215123, China*

[3]*University of Chinese Academy of Sciences, Beijing 100039, China*

[4]*e-mail: zhangdandan163@126.com*

**Corresponding author: jlu__jwy@63.com*

Received August 14, 2013; revised September 17, 2013; accepted October 27, 2013; posted October 28, 2013 (Doc. ID 195523); published November 22, 2013

A simple and efficient method to improve the internal and external quantum efficiency of phosphorescent organic light-emitting devices (PhOLEDs) is demonstrated, i.e., combining the localized surface plasmon (LSP) and optical scattering effects by introducing gold nanoparticles (NPs) coated by SiO_2 (named as Au@SiO_2). The effects of LSP and optical scattering on PhOLEDs are studied. The lifetime of the triplet exciton in the device is modified by surface plasmon coupling induced by Au@SiO_2 NPs, which results in increased internal quantum efficiency of the NP-containing devices. The optical scattering effect induced by Au@SiO_2 NPs enhances the light outcoupling efficiency of the PhOLEDs and is demonstrated by measuring the angularly resolved photoluminescence. As a result, a PhOLED with 101% improved efficiency and 21% reduced efficiency roll-off is achieved using the composite HTL.

OCIS codes: (230.3670) Light-emitting diodes; (230.0250) Optoelectronics; (290.5850) Scattering, particles; (250.5403) Plasmonics; (240.0310) Thin films.

http://dx.doi.org/10.1364/OL.38.005020

Tremendous interest has been focused on organic light-emitting devices (OLEDs) over the past few decades due to their potential applications for high-efficiency full-color flat-panel displays and solid-state lighting sources, with the advantages of low power consumption, excellent color gamut, fast response time, and flexibility [1,2]. In particular, the development of phosphorescent emission dyes highly improves the performance of OLEDs. The phosphorescent emitters can harvest both the singlet and triplet excitons, leading to the potential for achieving 100% internal quantum efficiency [3]. This important breakthrough has opened up the opportunity to fabricate highly efficient phosphorescent OLEDs (PhOLEDs). For example, the iridium complex based dyes doped into fluorescence host materials, such as fac-tris(2-phenylpyridine) iridium ($Ir(ppy)_3$) doped in 4, 4′ -bis(9-carbazolyl)-1, 1′ -biphenyl (CBP), have received much attention and efficient PhOLEDs are obtained [4]. Although an internal quantum efficiency of nearly 100% has been achieved, the problem of exciton quenching and poor light extraction efficiency (less than 20%) remains unresolved. Consequently, PhOLEDs still suffer from low efficiency limited by low light extraction efficiency and a dramatic decrease in EL efficiency at high current density and luminance, a behavior referred to as efficiency roll-off, which is predominantly ascribed to triplet–triplet annihilation (TTA) and triplet–polaron annihilation (TPA) due to the long radiative lifetime of the triplet excitons [5,6]. In an OLED under operation conditions, the exciton density is in proportion to the exciton lifetime [6]. Much effort has been devoted to reducing the efficiency roll-off of PhOLEDs [7–13]. One of the most important strategies is the introduction of metal nanoparticles (NPs) into the device to increase the spontaneous radiation ratio of the excitons and reduce the efficiency roll-off due to the effect of localized surface plasmon resonance (LSPR) [14–16]. However, the Au NPs were directly contacted by the emission layer in [15], which would result in exciton quenching near the bare Au NPs. Moreover, the optical scattering effect is weak due to the small size of the metal NPs in previous reports. Here, we introduced the Au NPs coated with silica shell, named Au@SiO_2, into the device. The SiO_2 shell helps to isolate bare Au NPs from electronic and chemical corrosion and prevent the direct injection of electrons into Au@SiO_2 NPs, which will lead to electron quenching or traping [17]. The Au@SiO_2 NPs possess much higher stability than that of bare Au NPs due to the barrier for NP agglomeration and impurity diffusion provided by the SiO_2 shell. The SiO_2 shell on the Au surface allows for the nearly unattenuated propagation of incident electromagnetic waves; therefore, it has a negligible influence on the optical properties of Au@SiO_2 NPs, and this is demonstrated by a theoretical simulation shown below. In addition, the efficiency of OLEDs containing SiO_2 NPs in HIL was highly improved due to the optical scattering effect of SiO_2 NPs on the light [18]. The composite HTL doped by Au@SiO_2 NPs presented here is suitable for integrating NPs for improved outcoupling via scattering and reducing the efficiency roll-off by LSPR. Consequently, we combine these two effects, LSPR and scattering, into the devices simultaneously and obtain highly efficient PhOLEDs.

In this work, we fabricated PhOLEDs containing ~60 – nm-diameter Au@SiO_2 core/shell NPs in PEDOT:PSS HIL. The diameter of the Au core is about 15 nm. The device performance is improved by the collaborative effects of optical scattering and LSPR induced by Au@SiO_2 NPs. Therefore, inspecting the performance of PhOLEDs with and without Au@SiO_2 NPs is of great

value to figure out the real mechanism of the synergic effect in PhOLEDs. Time-resolved photoluminescence (TRPL) measurements are used to study changes in the decay rate of triplet excitons of $Ir(ppy)_3$ doped into CBP (CBP:$Ir(ppy)_3$) due to interaction with Au@SiO_2 NPs. The optical scattering effect induced by Au@SiO_2 NPs on the device performance is analyzed.

PhOLEDs consisted of glass substrate coated with ITO/HIL (~50 nm) /CBP: $Ir(ppy)_3$ (30 nm)/1,3,5-Tri(1-phenyl-1H-benzo[d]imidazol-2-yl)phenyl (TPBi, 40 nm)/LiF (1.0 nm)/Al (200 nm). The PEDOT:PSS (Baytron PH) was used as received. The PEDOT:PSS (Baytron PH): Au@SiO_2 was used as the HIL with different Au@SiO_2 concentration. To realize NP-containing HTL, we first prepared the Au@SiO_2 NPs (~60 – nm in diameter) dispersion in alcohol with different concentration, and then mixed the Au@SiO_2 NPs solution with the PEDOT:PSS solution with volume ratios of 1:1. The Au@SiO_2 NPs solution with concentration of 2, 5, and 10 wt.% was used for devices A, B, and C, respectively. Device D as the control device was also fabricated with PEDOT:PSS as the HIL. The PEDOT:PSS and PEDOT:PSS: Au@SiO_2 films were spin coated on ITO at 3000 rpm and then annealed at 120°C for 30 min in a glove box (MBRAUN) to obtain a highly conductive layer. The thickness of all the HILs is about 50 nm by measuring the scanning electron microscope (SEM) of the HIL cross sections (data are not shown). The CBP: $Ir(ppy)_3$, TPBi, Li, and Al were deposited on the HIL successively by thermal evaporation at pressure below 4×10^{-6} Torr. The layer thickness and the deposition rate of the materials were monitored *in situ* using an oscillating quartz thickness monitor, and the deposition rates of TPBi and LiF were controlled to about 0.2 and 0.01 nm/s. The metal were controlled to about 0.5–1 nm/s. Glass substrates coated with ITO were carefully cleaned by scrubbing and sonication. The characteristics of current–voltage and luminance were measured by a programmable Keithley model 2400 power supply and a Minolta Luminance Meter LS-110, respectively, in air at room temperature. The spectra of the devices were measured with an Ocean Optics Maya 2000-Pro spectrometer. For all devices, no external package or encapsulation was applied after device fabrication. The morphology of QD was characterized by SEM (Hitachi S4800). TRPL measurements were carried out with an Edinburgh Instruments FL920 spectrometer. For the TRPL measurements, the samples were fabricated on quartz substrates and all the films were fabricated using the same technique described above. Various samples for TRPL measurements consisted of substrate/PEDOT:PSS: Au@SiO_2 (~50 nm)/CBP: $Ir(ppy)_3$ (30 nm). The HTLs were fabricated with the same method as the above and the concentration of the Au@SiO_2 NPs is controlled to 0%, 2%, 5%, and 10%.

Figure 1(a) shows the measured absorption spectra of the bare Au and Au@SiO_2 NPs as well as the simulated absorption spectrum of the Au@SiO_2. As can be seen, the absorption peak of the Au@SiO_2 NPs shifts to longer wavelength relative to that of bare Au NPs, which is due to the difference in refractive indices around Au NPs for bare Au NPs and Au@SiO_2 NPs. It is well known that changing this environment can affect the plasmon oscillation frequency due to the varying ability of the surface to accommodate the electron charge density and distribution in the Au NPs [19]. The simulated result for the absorption spectrum is in excellent agreement with the experimental one, which also demonstrates the successful preparation of Au@SiO_2 NPs. The inset shows the SEM image of the Au@SiO_2 NPs; the diameter of the NPs is about 60 nm. Figure 1(b) shows the schematic device structures with and without NPs, and the size is not to scale. Here, we also calculated the distribution of the field intensity of bare Au NPs and Au@SiO_2 NPs in the PEDOT:PSS layer on ITO substrate at the LSPR wavelength of 520 nm using the finite difference time-domain (FDTD). The transverse magnetic (TM) distributions around the Au NP were modeled for Au and Au@SiO_2 NPs as shown in Fig. 2. Here, z is defined as the light incident direction, and x is the polarization direction. As can be seen from these figures, the SiO_2

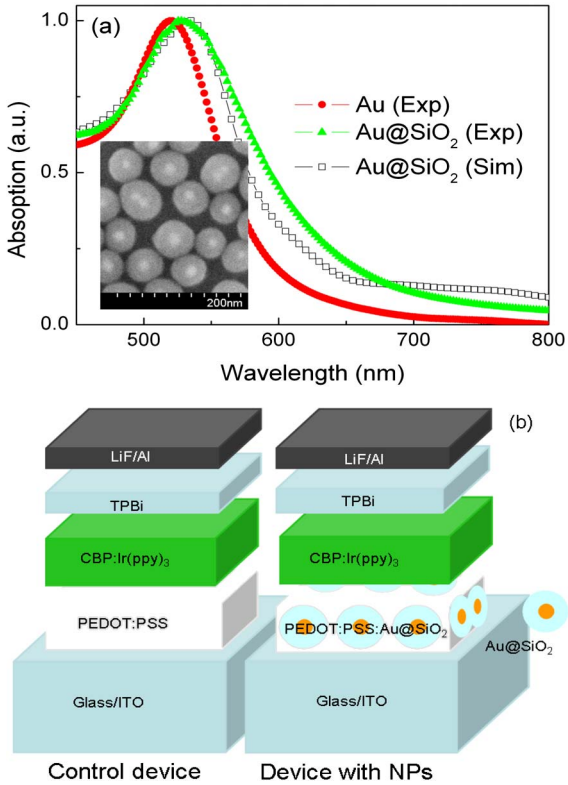

Fig. 1. (a) Measured (Exp) and simulated (Sim) absorption spectra of Au and Au@SiO_2 NPs; inset is the SEM image of Au@SiO_2 NPs. (b) Schematic device structures with and without Au@SiO_2 NPs. (Note: not to scale.)

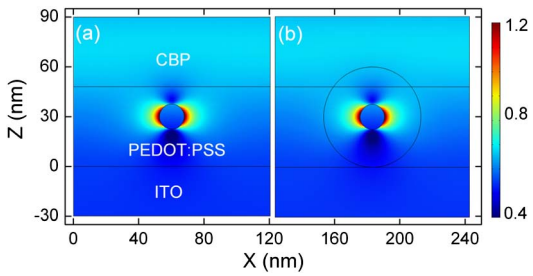

Fig. 2. Simulated electric field profile of transverse magnetic (TM) illumination of (a) Au NPs and (b) Au@SiO_2 NPs on the ITO substrate at the wavelength 520 nm.

shell on the Au surface allows for nearly unattenuated propagation of incident electromagnetic waves; therefore, it has a negligible influence on the optical properties of Au@SiO_2 NPs.

The current density–voltage characteristics of all the devices are shown in Fig. 3(a). We can see that the introduction of Au@SiO_2 NPs into the devices decreases the current density compared to that of the control device. This quite remarkable phenomenon is the larger current density is obtained with higher ratio of Au@SiO_2 NPs in PEDOT:PSS, which is also observed in [18]. We attribute it to the anisotropy in the conductivity for PEDOT:PSS such that in-plane conductivity values exceed the vertical conductivity as reported by Nardes *et al.* [20]. According to the report by Riedel *et al.*, the conductivity of the composite HIL of PEDOT:PSS doped by SiO_2 NPs is very different with different SiO_2 NPs concentration [18]. As reported by Riedel *et al.*, the decreased current density might be attributed to changes in the work function of the PEDOT:PSS: Au@SiO_2 layer, introducing a slight injection barrier to hole injection and thus decreasing the current density. Figure 3(b) shows the current density-efficiency curves of the four devices. A large improvement in efficiency is achieved in the device for a 5% Au@SiO_2 NPs device. Moreover, all PhOLEDs comprising NP-containing HTL show higher efficiency compared with the reference PhOLED. As discussed above, the improvement of the device performance does not originate from the different conductivity of the HILs. This might be attributed to the slight injection barrier to hole injection induced by the PEDOT:PSS: Au@SiO_2 layer, thus

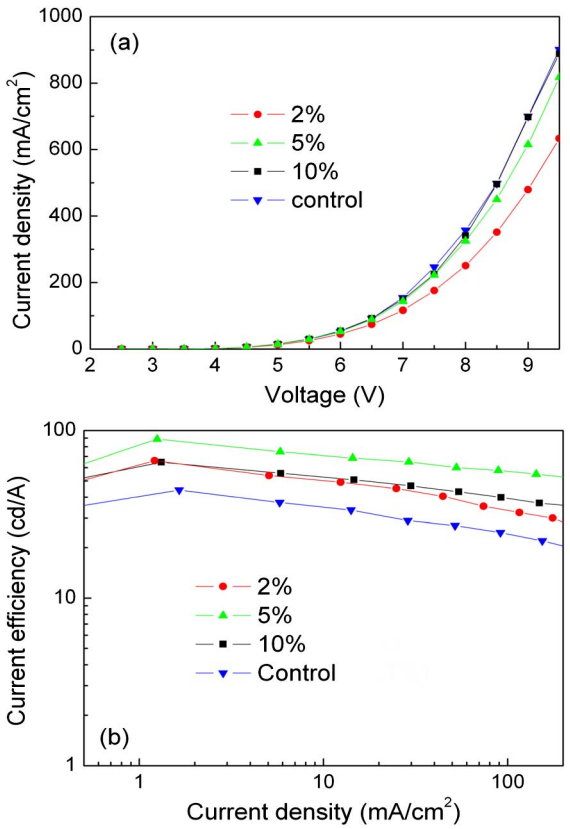

Fig. 3. (a) Voltage–current characteristics of all the devices and (b) current-efficiency curves of the devices.

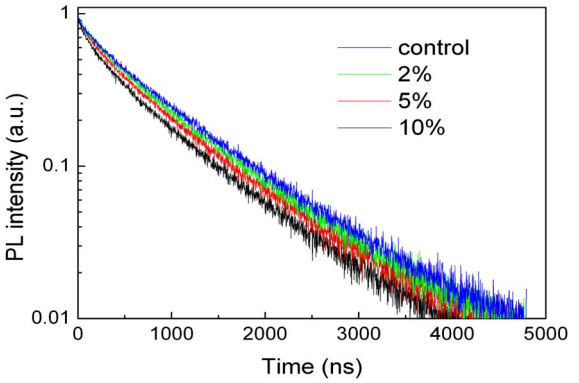

Fig. 4. PL intensity versus time from $Ir(ppy)_3$, following optical excitation by a 405 nm pulse.

improving the charge balance of the OLEDs. Further increasing the concentration of Au@SiO_2 NPs, the device efficiency is decreased, which may originate from the low hole-injection efficiency from HIL to the emissive layer.

Another salient feature is the reduced efficiency roll-off by introducing the Au@SiO_2 NPs into the devices. The lower efficiency roll-off (from the peak efficiency to that under the current density of 100 mA/cm^2) of 36% is obtained for device B compared to that of 46% for the control device, which is attributed to the LSPR effect induced by Au@SiO_2 NPs. In order to explain this, we carried out the measure for the lifetime of $Ir(ppy)_3$, and the results are shown in Fig. 4. As can be seen, the lifetime of the $Ir(ppy)_3$ excitons containing Au@SiO_2 NPs is shortened; the higher the concentration of Au@SiO_2 NPs in PEDOT:PSS, the shorter the lifetime of $Ir(ppy)_3$ excitons. The LSPR peak of 520 nm is well matched with the emission peak of 512 nm from $Ir(ppy)_3$. The radiative rate of $Ir(ppy)_3$ excitons is accelerated due to the interaction with LSPR, consequently reducing the exciton TTA possibility and efficiency roll-off. However, the efficiency roll-off of the device containing 10% Au@SiO_2 NPs is not obviously reduced although the lifetime of $Ir(ppy)_3$ excitons in this device is the most shortened. We attribute this to the large roughness of PEDOT:PSS for the 10% NPs layer. As we know, large roughness will result in large leakage current in the OLEDs. In addition, it is valuable to note the emission profile of the different devices. As shown in Fig. 5, according to the NP concentration, they reveal a changed emission characteristic. An

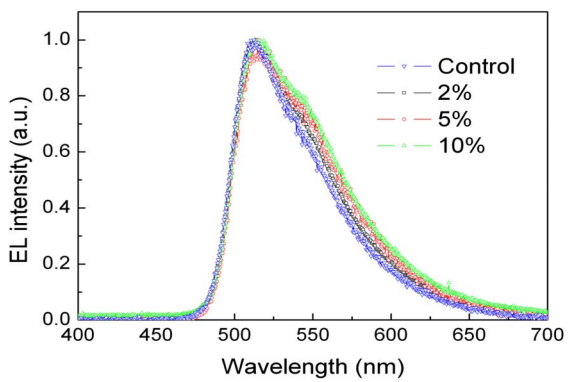

Fig. 5. EL spectra of all the devices at the voltage of 6 V.

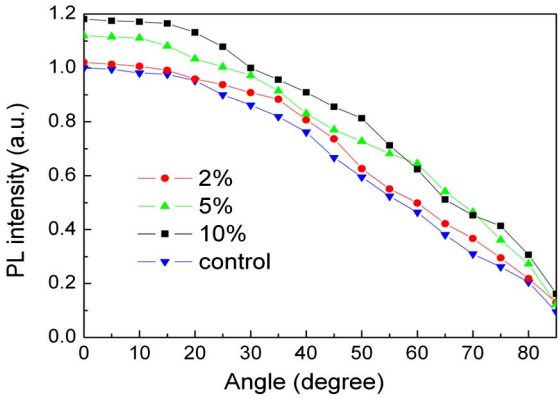

Fig. 6. Angularly resolved photoluminescence of all samples.

enhanced emission from 530 to 570 nm is observed, and a similar trend was reported previously [14]. This enhancement is attributed to the effect of LSPR induced by Au@SiO_2 on the device emission, which depends strongly on the concentration of NPs inside the HIL.

In addition, we attribute the other contribution to PL enhancement to the scattering effect induced by Au@SiO_2 NPs. Here, the effect of optical scattering of Au@SiO_2 NPs on the outcoupling should be estimated. In order to find out whether this enhancement is due to optical effects, we measured the angularly resolved PL as shown in Fig. 6, which is normalized to the sample without Au@SiO_2 NPs at normal direction. The samples for PL measurement consisted of ITO substrate/HIL (50 nm)/CBP(20 nm)/CBP: $Ir(ppy)_3$ (35 nm). The HIL has the same structure as the corresponding device as described above. The 20 nm neat CBP spacer is used to eliminate the effect of the LSPR of Au@SiO_2 NPs. From Fig. 2(b), we can see the influence of NPs on the electric field 20 nm away from the Au@SiO_2 NP surface is negligible. The excited light (405 nm) is incident from the CBP:$Ir(ppy)_3$ side, and the light (512 nm) emitted from the sample was collected from ITO. Here, all the PL intensity is increased with the increasing concentration of Au@SiO_2 NPs in PEDOT:PSS. Thus we deduce that enhanced outcoupling plays an important role in enhancing the device performance. The conflict between the PL results and the device efficiency, i.e., the device for 10% Au@SiO_2 NPs does not possess the highest efficiency, probably originated from the different electronic performance as discussed above, and a similar phenomenon is also observed in [18]. In addition, we measured the angular PL without the 20 nm neat CBP, and the integrated PL intensity is increased by 81%, which partly demonstrates a similar enhancement for external quantum efficiency.

In conclusion, we fabricated PhOLEDs containing ~60 – nm-diameter Au@SiO_2 NPs in HIL. A very high improvement of 101% in the peak current efficiency is achieved for the $Ir(ppy)_3$-based PhOLED. The efficiency roll-off (from the peak efficiency to that under the current density of 100 mA/cm^2) is reduced from 46% to 36%. The device performance enhancement mostly originated from the collaborative effects of scattering and LSPR induced by Au@SiO_2 NPs. In addition, the more balanced charge injection due to the introduction of Au@SiO_2 NPs also has a large contribution to the enhancement of the device efficiency. The composite HIL presented here provides a new design option in OLEDs concerning the adjustment of the cavity thickness, the conductivity, and the scattering properties.

This work was supported by the program of the National Natural Science Foundation of China (Nos. 61205025, 61275197).

References

1. B. W. D'Andrade and S. R. Forrest, Adv. Mater. **16**, 1585 (2004).
2. S. Reineke, F. Lindner, G. Schwartz, N. Seidler, K. Walzer, B. Lüssem, and K. Leo, Nature **459**, 234 (2009).
3. C. Adachi, M. A. Baldo, M. E. Thompson, and S. R. Forrest, J. Appl. Phys. **90**, 5048 (2001).
4. Z. W. Liu, M. G. Helander, Z. B. Wang, and Z. H. Lu, Org. Electron. **10**, 1146 (2009).
5. M. A. Baldo, C. Adachi, and S. R. Forrest, Phys. Rev. B **62**, 10967 (2000).
6. S. Reineke, K. Walzer, and K. Leo, Phys. Rev. B **75**, 125328 (2007).
7. J. W. Kang, S. H. Lee, H. D. Park, W. I. Jeong, K. M. Yoo, Y. S. Park, and J. J. Kim, Appl. Phys. Lett. **90**, 223508 (2007).
8. S. H. Kim, J. Jang, K. S. Yook, and J. Y. Lee, Appl. Phys. Lett. **92**, 023513 (2008).
9. T. Zheng, W. C. H. Choy, C. L. Ho, and W. Y. Wong, Appl. Phys. Lett. **95**, 133304 (2009).
10. S. Reineke, G. Schwartz, K. Walzer, and K. Leo, Appl. Phys. Lett. **91**, 123508 (2007).
11. S. Reineke, G. Schwartz, K. Walzer, M. Falke, and K. Leo, Appl. Phys. Lett. **94**, 163305 (2009).
12. F. X. Zang, T. C. Sum, A. C. H. Huan, T. L. Li, W. L. Li, and F. Zhu, Appl. Phys. Lett. **93**, 023309 (2008).
13. L. M. Zhang, B. Li, L. Y. Zhang, and Z. M. Su, ACS Appl. Mater. Interfaces **1**, 1852 (2009).
14. W. Y. Ji, L. T. Zhang, and W. F. Xie, Opt. Lett. **37**, 2019 (2012).
15. A. Choulis, M. K. Mathai, and V. Choong, Appl. Phys. Lett. **88**, 213503 (2006).
16. Y. Su, Y. Ke, S. Cai, and Q. Yao, Light: Sci. Appl. **1**, e14 (2012).
17. M. D. Brown, T. Suteewong, R. S. Kumar, V. D'Innocenzo, A. Petrozza, M. M. Lee, U. Wiesner, and H. J. Snaith, Nano Lett. **11**, 438 (2011).
18. B. Riedel, Y. Shen, J. Hauss, M. Aichholz, X. Tang, U. Lemmer, and M. Gerken, Adv. Mater. **23**, 740 (2011).
19. G. Xu, Y. Chen, M. Tazawa, and P. Jin, Appl. Phys. Lett. **88**, 043114 (2006).
20. A. Nardes, M. Kemerink, R. Janssen, J. Bastiaansen, N. Kiggen, B. Langeveld, A. Van Breemen, and M. de Kok, Adv. Mater. **19**, 1196 (2007).